NPS-MAE-10-006

NAVAL POSTGRADUATE SCHOOL

MONTEREY, CALIFORNIA

Direct Manufacturing of CubeSat Using 3-D Digital Printer and Determination of Its Mechanical Properties

by

Young W. Kwon, Luke N. Brewer, Rudolf Panholzer,
Daniel J. Sakoda, and Chanman Park

December 2010

Approved for public release; distribution is unlimited.

Prepared for: Defense Advanced Research Projects Agency (DARPA)
Defense Science Office, Arlington, VA 22203-1714

THIS PAGE INTENTIONALLY LEFT BLANK

NAVAL POSTGRADUATE SCHOOL
Monterey, California 93943-5000

Daniel T. Oliver
President

Leonard A. Ferrari
Executive Vice President and
Provost

This report was prepared for and funded by the Defense Advanced Research Projects Agency (DARPA), Arlington, VA 22203.

This report was prepared by:

Young W. Kwon Distinguished Professor	Luke N. Brewer Associate Professor	Rudolf Panholzer Professor & Chairman of Space Systems Academic Group
Daniel J. Sakoda Research Associate		Chanman Park Research Associate

Reviewed by:

Knox T. Millsaps, Chair
Mechanical & Aerospace
Engineering Department

Released by:

Karl A. van Bibber
Vice President and
Dean of Research

THIS PAGE INTENTIONALLY LEFT BLANK

REPORT DOCUMENTATION PAGE

Form Approved
OMB No. 0704-0188

1. REPORT DATE *(DD-MM-YYYY)*	2. REPORT TYPE	3. DATES COVERED *(From - To)*
31-12-2010	Technical Report	Oct - Dec 2010

4. TITLE AND SUBTITLE

Direct Manufacturing of CubeSat Using 3-D Digital Printer and Determination of its Mechanical Properties

5a. CONTRACT NUMBER
11-F836

5b. GRANT NUMBER

5c. PROGRAM ELEMENT NUMBER

6. AUTHOR(S)

Young W. Kwon, Luke N. Brewer, and Rudolf Panholzer, Daniel J. Sakoda, Chanman Park

5d. PROJECT NUMBER

5e. TASK NUMBER

5f. WORK UNIT NUMBER

7. PERFORMING ORGANIZATION NAME(S) AND ADDRESS(ES)

Naval Postgraduate School
Dept. of Mechanical &
Aerospace Engineering
700 Dyer Rd
Monterey, CA 93943

8. PERFORMING ORGANIZATION REPORT NUMBER
NPS-MAE-10-006

9. SPONSORING / MONITORING AGENCY NAME(S) AND ADDRESS(ES)
Defense Advanced Research Projects Agency
9701 N. Fairfax Dr.
Arlington, VA 22203

10. SPONSOR/MONITOR'S ACRONYM(S)
DARPA

11. SPONSOR/MONITOR'S REPORT NUMBER(S)

12. DISTRIBUTION / AVAILABILITY STATEMENT
Approved for public release; distribution is unlimited.

13. SUPPLEMENTARY NOTES

14. ABSTRACT

A 3-D digital prototype printer has been considered for direct digital manufacturing of components because this technology has many benefits compared to conventional manufacturing technologies. In order to assess the applicability of the direct digital fabrication to a critical structural component, mechanical properties of the digitally fabricated component should meet the design or performance requirements. Furthermore, it is necessary to be able to predict the mechanical properties of the fabricated component based on the input parameters of the 3-D digital printer. The present project measured the mechanical properties (i.e. strength and stiffness) of samples fabricated from a 3-D digital printer as a function of processing parameters, determined predictive model connecting the input parameters to the 3-D digital printer and mechanical properties of the fabricated samples by using a statistical design of experiments and multivariate regression, validated the model using crush-strength experiments on the NPS CubeSat structure, and to hosted the CubeSat challenge.

15. SUBJECT TERMS
Direct Manufacturing, 3-D Printer, Mechanical Properties

16. SECURITY CLASSIFICATION OF: Unclassified			17. LIMITATION OF ABSTRACT	18. NUMBER OF PAGES	19a. NAME OF RESPONSIBLE PERSON Young W. Kwon
a. REPORT	b. ABSTRACT	c. THIS PAGE			19b. TELEPHONE NUMBER *(include area code)*
UU	UU	UU	UU	27	831-656-3468

Standard Form 298 (Rev. 8-98)
Prescribed by ANSI Std. Z39.18

THIS PAGE INTENTIONALLY LEFT BLANK

ABSTRACT

A 3 -D di gital pr ototype pr inter h as be en considered for di rect digital manufacturing o f c omponents be cause t his t echnology ha s m any be nefits c ompared t o conventional manufacturing technologies. In order to assess the applicability of the direct digital f abrication to a c ritical s tructural c omponent, me chanical p roperties o f th e digitally fabricated component s hould m eet t he de sign or pe rformance r equirements. Furthermore, i t i s n ecessary t o b e able t o p redict t he m echanical p roperties o f t he fabricated co mponent b ased on t he i nput pa rameters of t he 3 -D di gital pr inter. T he present project measured the mechanical properties (i.e. strength and stiffness) of samples fabricated from a 3 -D digital printer as a function of processing parameters, determined predictive m odel c onnecting t he i nput pa rameters t o t he 3 -D d igital p rinter a nd mechanical p roperties of t he f abricated s amples b y u sing a s tatistical d esign o f experiments a nd m ultivariate r egression, v alidated t he m odel us ing c rush-strength experiments on the NPS CubeSat structure, and to hosted the CubeSat challenge.

THIS PAGE INTENTIONALLY LEFT BLANK

TABLE OF CONTENTS

THIS PAGE INTENTIONALLY LEFT BLANK

I. Introduction

Direct digital manufacturing (DDM) is science imitating art, science fiction movies to be exact. The ability to tell a computer that we want a certain object and have the computerized machine simply produce the requested item is reminiscent of the technological wonders that captivated us in the Star Trek movies. Technology being inspired by literature has happened several times with the submarine, *Nautilus,* from the novel Twenty Thousand Leagues under the Sea being a prime example.[1] The *U.S.S. Nautlius* was successfully launched in 1954. Fortunately, direct digital manufacturing is also on the path from science fiction to practical reality. This project intentionally examines where we are on that path for the case of plastic CubeSat structures.

DDM builds upon the now widely used rapid prototyping equipment for fabricating polymeric, ceramic, and metallic structures using a variety of printer technologies.[2-4] Initially, these technologies were developed to rapidly produce custom parts for building mechanical prototypes. Over the past several years, much work has been done to extend both the underlying science and technological capabilities of the DDM approach towards full production of end products, comparable or even superior to traditional manufactured components. Parametric studies on acrylonitrile butadi- ene styrene (ABS P 400) structures using fused deposition modeling (FDM) have been performed using statistical design of experiments and multivariate regression.[5, 6] These studies found that processing parameters, such as layer thickness and raster angle, did result in distinct changes in mechanical behavior for this polymer system. Other recent work by Masood et al. has begun to examine the processing-mechanical property relationships in FDM-produced polycarbonate components.[7]

This project has extended this field in three ways. We have performed a detailed, parametric study of the processing-property relationships in the polycarbonate polymer system. Second, we have taken these results and fabricated, predicted, and tested the mechanical behavior of larger, more complex structures. Finally we supported the DARPA DMACE Challenge and used it as a vehicle for assessing our ability to successfully predict the mechanical behavior of digitally manufactured, complex structures.

The specific objectives of this research program were:

(1) to measure the mechanical properties (i.e. strength and elastic modulus) of samples fabricated from a 3-D digital printer as a function of processing parameters

(2) to determine predictive model connecting the input parameters to the 3-D digital printer and mechanical properties of the fabricated samples by using a statistical design of experiments and multivariate regression

(3) to validate this model using crush-strength experiments on the NPS CubeSat structure

(4) to host the CubeSat portion of the DMACE challenge.

This report describes the research that has met these objectives and discusses what has been learned in our quest to digitally manufacture complex, three-dimensional structures.

THIS PAGE INTENTIONALLY LEFT BLANK

II. Processing-Mechanical Property Relationships in Direct Digitially Manufactured Polycarbonate

In this portion of the project, a series of statistically designed specimens were produced to correlate the key processing parameters of the DDM process with mechanical properties of the resultant material. Ideally, we would find little or no correlation, meaning that production of complex shapes is insensitive to the exact processing conditions. Alternatively, it is crucial that we develop the response surfaces, or system identifications, that quantitatively predict the mechanical properties as a function of processing conditions.

1. Production of samples

In order to efficiently assess the importance of processing parameters on mechanical properties of digitally manufactured polycarbonate, statistical design of experiments was employed. Four processing variables were identified as most important: tip size (TS), build angle (BA), raster angle (RA), and time in furnace (K). Table 1 displays the range of these values. A full factorial design with two levels for each factor and 1 replicate at each point was employed in order to assess the effects of all primary factors and their interactions. The replicates were included in the design in order to measure the pure error of the measurement system. This experimental design resulted in 32 specimens for compression testing. It was deemed likely that the mechanical response of the polycarbonate would be different in tension versus compression. Eight additional tensile samples were produced using the larger of the two tip sizes and one hour in the furnace to check this assumption.

The geometries of the compression and tension specimens were based upon standards used in the mechanical testing of polymers. The compression specimens (Figure 1) were rectangular parallelepipeds with a square cross section. They were approximately 50 millimeters (2 inches) in length and 12 millimeters (0.5 inches) in width and thickness. This aspect ratio is within the window specified by the D 695 standard and allows for stable compression testing.[8] Several geometries are allowed for tension specimens under the D638 standard.[9] We chose the type I specimen as it is the most commonly used and best fit our mechanical testing equipment (Figure 2).

Table 1. Input Variables for 3-D Digital Printer.

Variables	*Range of Parameter*
Tip Size	0.178mm (T12)-0.254 mm (T16)
Raster Angle	0 -90 degrees
Building Angle	0-90 degrees
Time in Furnace	1 or 10 hrs

The naming convention for samples would list a specimen with a 0.178 tip size, a zero degree raster angle, a ninety degree build angle, and 10 hours in the furnace as (T12R0B90K).

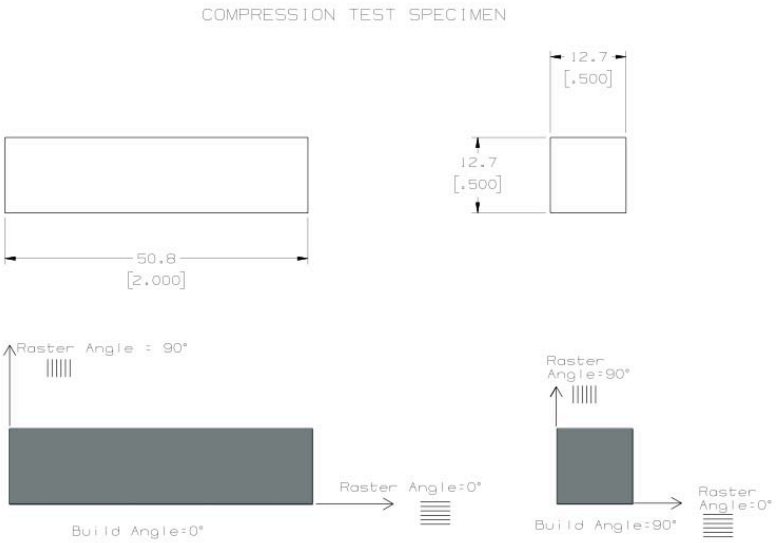

Figure 1. Geometry of compression specimens, based upon ASTM standard D695.

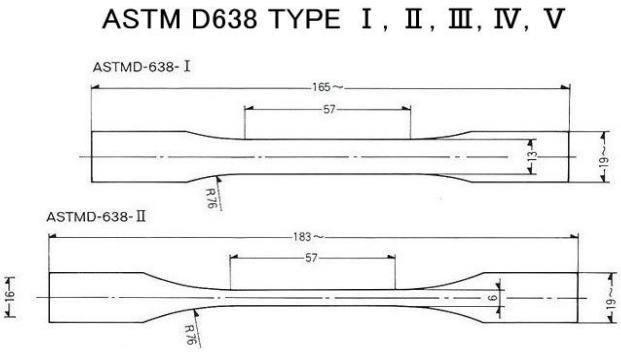

Figure 2. Geometry of tension specimens, based upon ASTM standard D638.

A Stratasys FORTUS 400mc was used to build the test specimens and the CubeSat parts. The FORTUS 400mc machine employs fused deposition modeling (FDM) for additive manufacturing of three-dimensional parts from computer-aided design (CAD) geometry. All specimens were made from polycarbonate material. A three dimensional (3D) geometry is brought into the 3D printer software application and rotated for the desired build orientation. The software then slices horizontal build planes and creates tool paths for each slice of the part based on the configuration of the machine. Once individual part tool path jobs are complete, the print jobs are arranged on the build area and sent to the machine.

The following figure illustrates the build for the compression specimen. In this example, the longitudinal dimension, or load direction of the specimen lies in the X-direction of the build plane, and a raster angle of 0° is defined. The outer edges are defined by contour lines, and the interior fill area is defined by raster lines. During the tool path generation, machine parameters can be defined. For this study, the raster angle

used for each slice of the part was defined as either 0° or 90°, as shown in Figure 3. The build angle relates to the orientation of the part geometry for the build, generally the part longitudinal axis, or load direction, with respect to the build direction. In Figure three, the compression axis is perpendicular to the build direction, giving a build angle of 90 degrees.

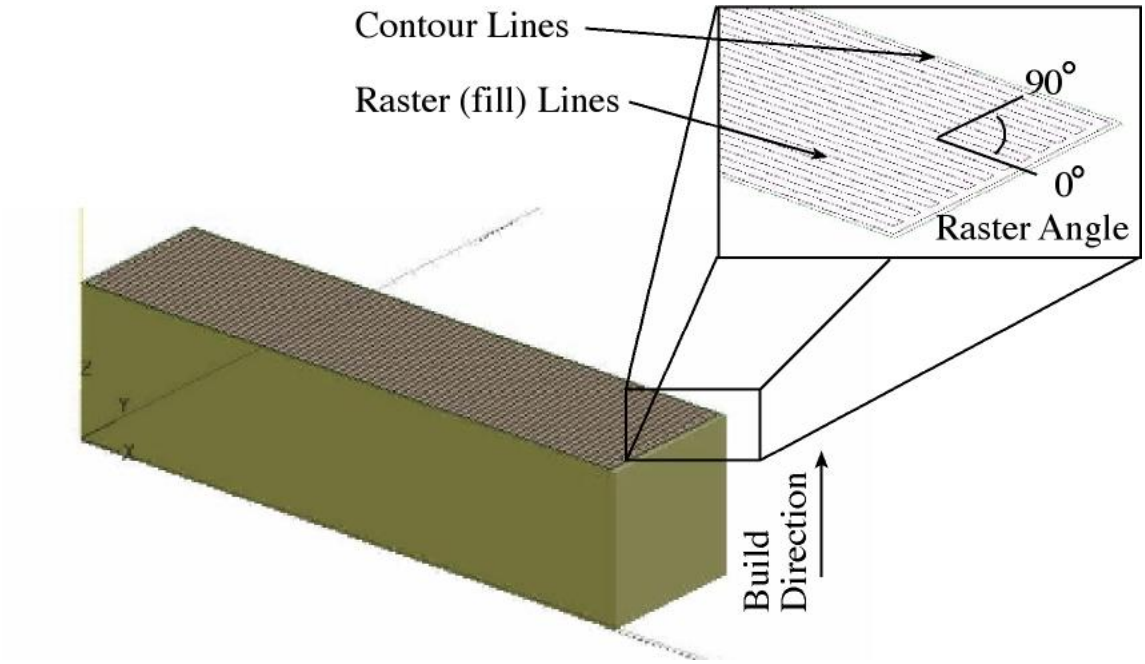

Figure 3. Illustration of Raster Angle of 0 degrees and build angle of 90 degrees.

2. Mechanical testing

Compression testing was done using a SATEC MII-20UD mechanical test frame with the Bluehill Advanced Test Module control software. The displacement rate was 1.3mm/min. The load was measured using a 50 kN load cell. A tabular summary of all results is listed in Appendix A for this report.

Tensile testing was done using an Instron Model 4507 mechanical test frame, also with Bluehill Advanced Test Module control software. The displacement rate was 2 mm/min. The load was measured using a 10 kN load cell. The displacement was measured using the cross head displacement with a resolution of less than 1 micron. A tabular summary of all results is listed in the Appendix A for this report.

The mechanical properties in compression varied significantly with processing conditions. This result confirms that there is a non-zero correlation between processing conditions and observed mechanical properties, thus meaning that parametric analysis of DDM produced parts is necessary for accurate prediction of their mechanical response.

In particular, we examine the Young's modulus, the linear slope during initial loading, and the maximum stress in compression. As is discussed later in the report, the Young's modulus is a primary parameter for predicting for predicting failure loads from buckling of structures without stress concentration, while the maximum stress (i.e. fracture strength) is important in predicting the failure load of the structure resulting from stress-initiated failure. The smaller tip size (0.178mm) showed a large range of maximum stress values, 21.25MPa, or 33 percent of the mean (64.04 MPa). Likewise, the range of the Young's modulus was 26 percent of the mean (2.67GPa). The values for the larger tip size also showed measurable variation, but not as large as for the smaller tip size.

The difference between mechanical behavior in tension versus compression was qualitatively large. While Young's modulus has a similar definition in the two deformation modes, the Young's moduli in tension were less than half of the value in compression (mean value of 1.16 GPa in tension compared with 2.70GPa in compression). The nature of maximum stress in tension is different in tension than in compression. Nonetheless, the tensile maximum stress did produce results that matched the compression results for one set of processing conditions. However, the maximum stress in tension was strongly correlated with processing orientation and had a range, which was 109 percent of the mean value (39.28MPa).

3. **Statistical Analysis**

Least squares analysis was used to analyze the variance (ANOVA) of the mechanical properties data. The commercial software JMP 8.0 was used to perform these analyses. Two statistical tasks were performed in analyzing the data. First, we used ANOVA and t-tests to determine the statistical significance of processing conditions in describing the mechanical behavior of the material. Second, we used parameter estimates to create response surfaces with which to predict the mechanical properties as a function of processing conditions. All of the statistical analysis results are found in Appendix B at the end of this report.

For the compression data, not all of the processing parameters were statistically significant. The exact significance of processing parameters was dependent upon the mechanical property. Statistical significance was determined by t-ratio values at the 95% confidence level (t-ratio ≥ 2, p-value ≤ 0.05). For the maximum stress in compression, tip size, build angle, and raster angle were all significant (Table 2). Bake was not a significant parameter, nor were any of its interactions. The interaction of tip size with raster angle was also not significant to the 95% confidence level. For the Young's modulus in compression, neither tip size nor bake were significant factors. For both maximum stress and Young's modulus, the models left a relatively significant portion of the variance unexplained (20% and 32%, respectively). This result means that while the factors identified are significant, accurate prediction of all of the data would require other, unidentified factors or a non-linear model.

Table 2. Estimate and statistical significance of parameters for describing the maximum stress in compression.

Term	Estimate	Std Error	t Ratio	Prob>|t|
Intercept	65.927188	0.559588	117.81	<.0001*
Tip Size(0.178,0.254)	1.8871875	0.559588	3.37	0.0023*
Raster Angle(0,90)	-3.000937	0.559588	-5.36	<.0001*
Build Angle(0,90)	-3.377812	0.559588	-6.04	<.0001*
Tip Size*Build Angle	2.3934375	0.559588	4.28	0.0002*
Raster Angle*Build Angle	1.4090625	0.559588	2.52	0.0183*

For the tension experiments, bake and tip size were not included in the experiments, only build angle and raster angle. These two factors and their interaction described over 95 percent of the variance in the data. The build angle was clearly the most important parameter in describing the variance of this limited data set.

Response surfaces were created using the estimates from the least squares analysis of the data (Figure 4). The equations for these surfaces are listed below.

Maximum Stress in Compression= 65.9+1.89*TS-3.00*RA-3.38*BA+2.39*TS*BA+1.41*RA*BA (1)

Young's Modulus in Compression=2.70-0.095*RA-0.043*BA+0.078*RA*BA (2)

Maximum Stress in Tension= 39.3-3.94*RA-17.1*BA+2.42*RA*BA (3)

Young's Modulus in Tension=1.16-0.035*RA-0.0675*BA+0.02*RA*BA (4)

Where TS= tip size, RA=raster angle, BA=build angle. Bake time, signified by "K" was not a significant factor for any response. For the maximum stresses in compression and tension the data has been plotted using a tip size of 0.254mm. These surfaces could be used for interpolative prediction of the mechanical properties based on processing conditions chosen within the range of parameters given in Table 1. Given the relatively low R-squared value for the models in compression, it is likely that there is a more complex curvature to these surfaces than is represented in Figure 4. This curvature could be better determined by additional experiments using processing parameters in the middle of the space. Nonetheless, these response surfaces can be used as the quantitative connection between processing parameters, the mechanical properties of the material produced, and the expected mechanical behavior of manufactured components discussed in the next section.

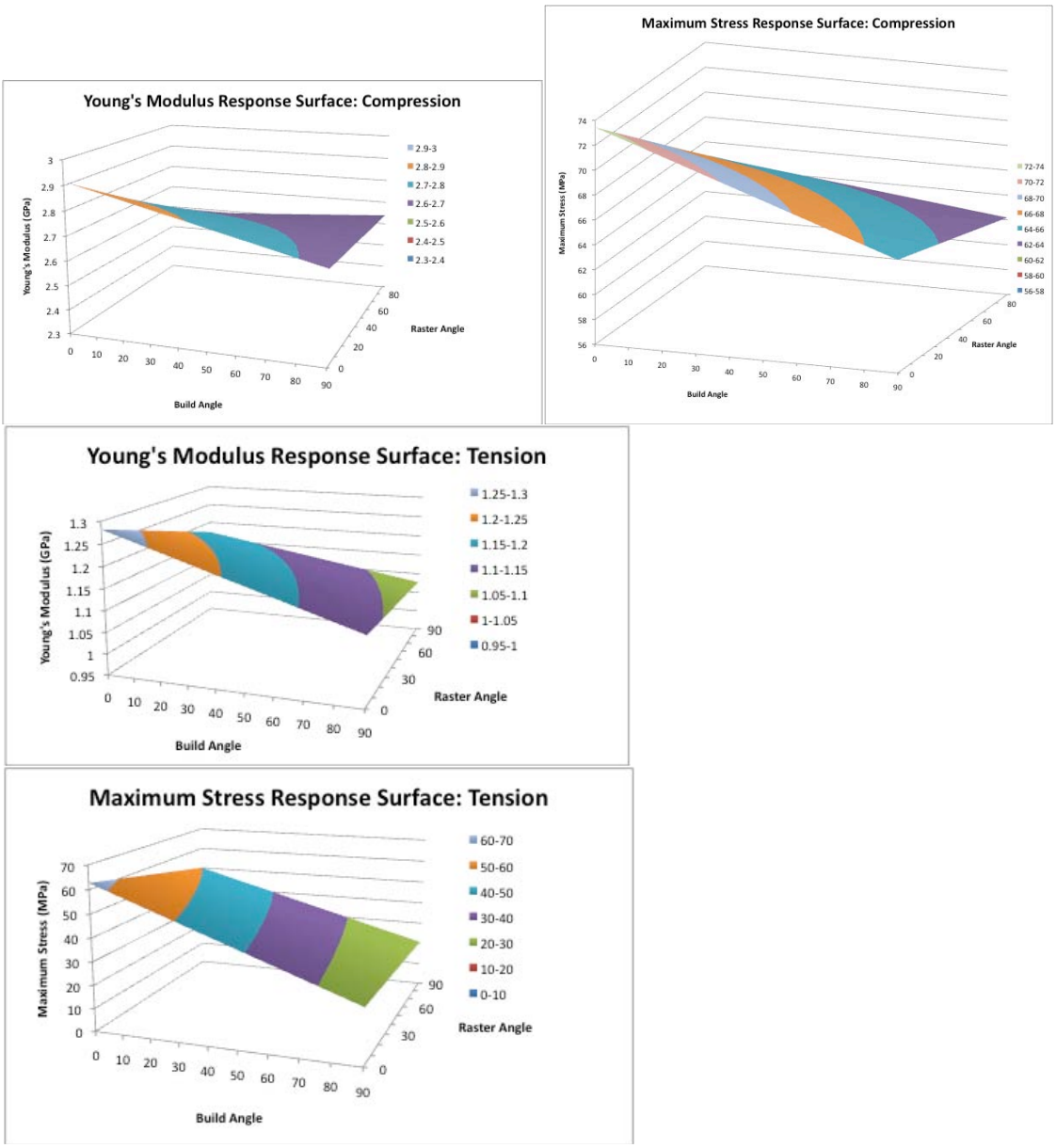

Figure 4. Response Surfaces based on estimates from least squares analysis of the data. A.) Young's modulus in compression, B. Maximum stress in compression, C.) Young's modulus in tension, D.) Maximum stress in tension.

III. Direct Digital Manufacturing of CubeSat Structures

The component chosen for DDM was a CubeSat. These structures are miniature satellites used for space research, primarily in academia. The basic structure is one liter in volume, 10cm by 10cm by 10cm. These structures could immediately benefit from DDM as each one is designed by an individual research team for a specific space experiment. The flexibility to change the design and rapidly manufacture to unique and exact tolerances is extremely helpful.

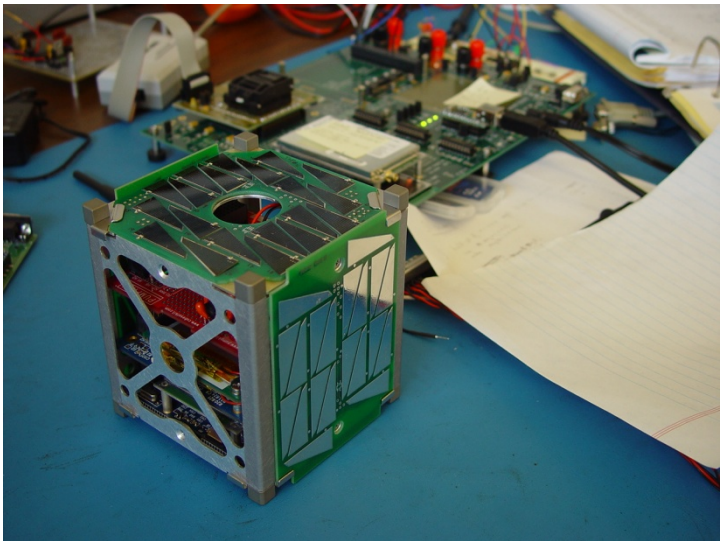

Figure 5. CubeSat used for satellite research in the Space Systems Academic Research Group at the Naval Postgraduate School.

We produced two types of CubeSats for basic analysis and to provide the "training data" described in section IV. The first CubeSat (CS1) was a simple, open-topped box 10cm on each side with 5mm thick walls. The second CubeSat (CS2) was the same as CS1 except that CS 2 had it had a four-by-four array of squares on all four sides. For both CS1 and CS2, the CubeSats were produced with TS=0.254mm, RA=90, BA=0, and no bake. Several replicates of each designed were produced.

The crushing load of the CubeSats was determined using the same instrumentation as described above for the basic compression tests. CS2 is shown in the mechanical test frame in Figure 6. Note the top mounting surface makes use of spring-loaded, spherical bearing surface to ensure proper alignment during compression. The crushing load was taken to be the maximum force during compression.

Figure 6. CS2 structure mounted for compression testing.

The mechanical response of the CubeSat structures had both similarities and differences (Figure 7). Both structures had a well defined yield point. Both structures also had brittle failure mode at maximum load, as evidence by the vertical drop in load. Both structures exploded into many pieces upon failure. The CS2 lattice structure has a smoother after-yield profile than the CS1 solid structure, which showed serrations in load after initial yielding. These serrations are believed to be from initial crack generation prior to final failure. The discontinuity in the load-displacement curve at low loads is likely from compliance in the load train.

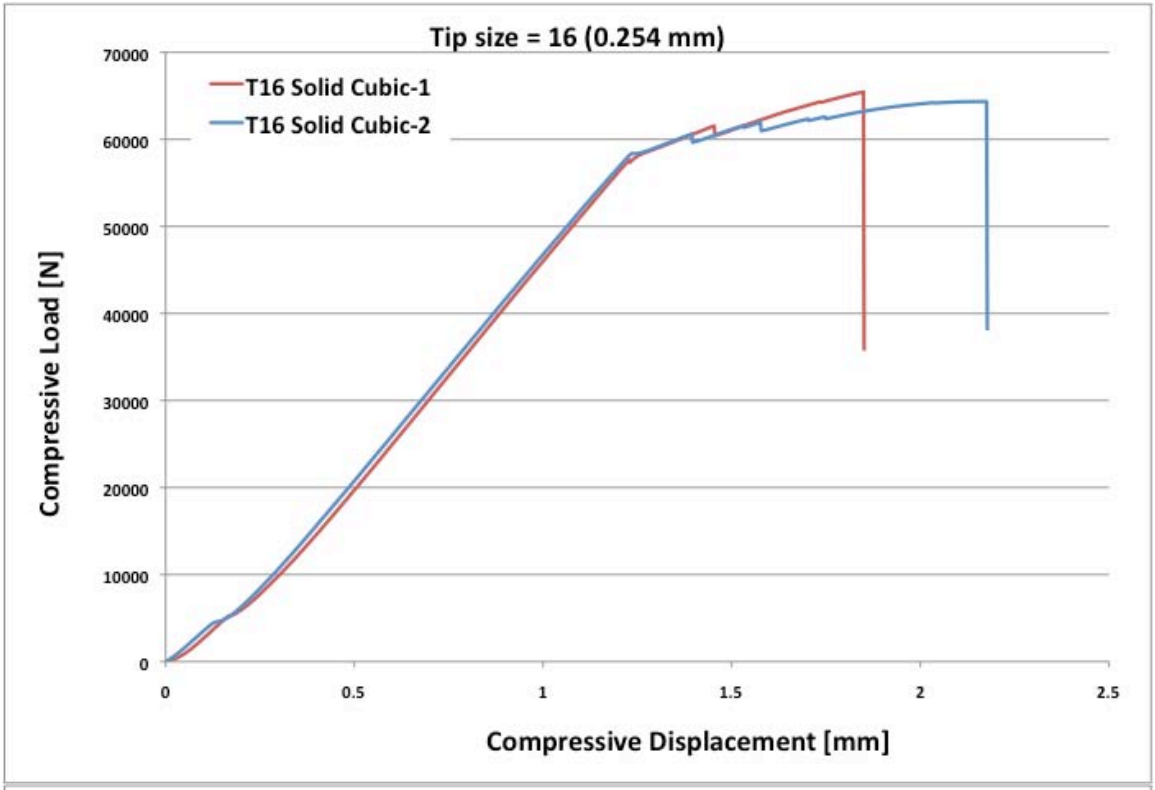

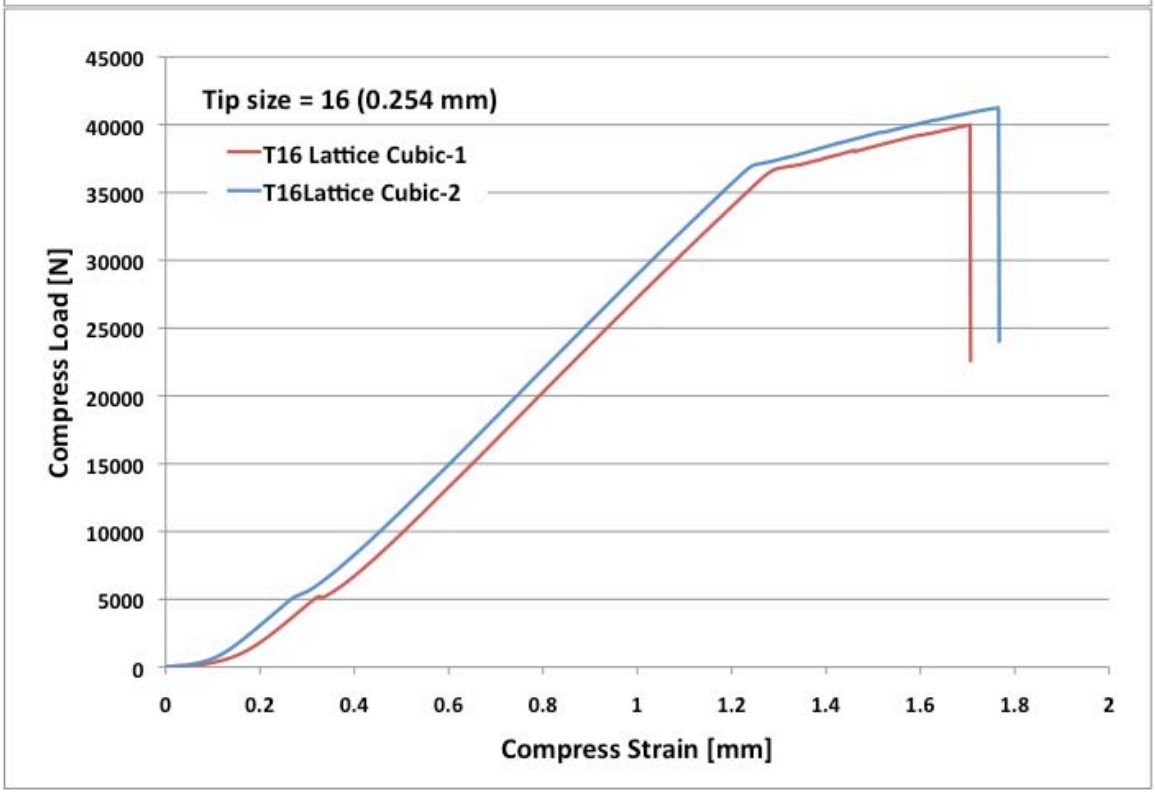

Figure 7 Load-displacement curves for CS1 solid (top) and CS2 lattice (bottom) structures.

Finite element analysis (FEA) is a good tool for predicting the strength and stiffness of complex structures. As a result, FEA was used to predict and analyse the crushing response of the CS1 and CS2 structures. One has solid walls while the other has lattice-shaped walls as shown in Figure 8. As described above, both structures are 10 cm x 10 cm x 10 cm for the outside dimensions and a have a uniform wall thickness of 5 mm. The ratio of the wall length to the thickness is approximately 20. This ratio means that when the cubes are compressed, they will fail by buckling of the walls. One of the simplest mechanics analyses of this kind of deformation is linear buckling analysis, which is an eigenvalue analysis. Linear buckling analysis depends only upon the elastic modulus of the material and not upon the strength.

A finite element mesh for the CS2 structure in Figure 6 is shown in Figure 8. The geometry was imported from the CAD file of the 3-D printer and tetrahedral element shapes were used for the mesh. There were 40,312 elements with 75,417 nodes in the model. As the boundary condition, the bottom surface of each cube was assumed to be constrained from displacements in all directions. On the other hand, tangential displacements on the top surface were constrained while the compressive force was applied to the normal to the top surface. Such boundary conditions were based on the assumption of no slip between the top/bottom surfaces and the surface of the mechanical testing machine as shown in Figure 6. Certainly, this is an idealized boundary condition. As discussed in the statistical analysis in section II, the material elastic modulus depends upon the raster and build angles. However, for these initial FEA simulations, the finite element models assume uniform elastic modulus as the first order of approximation.

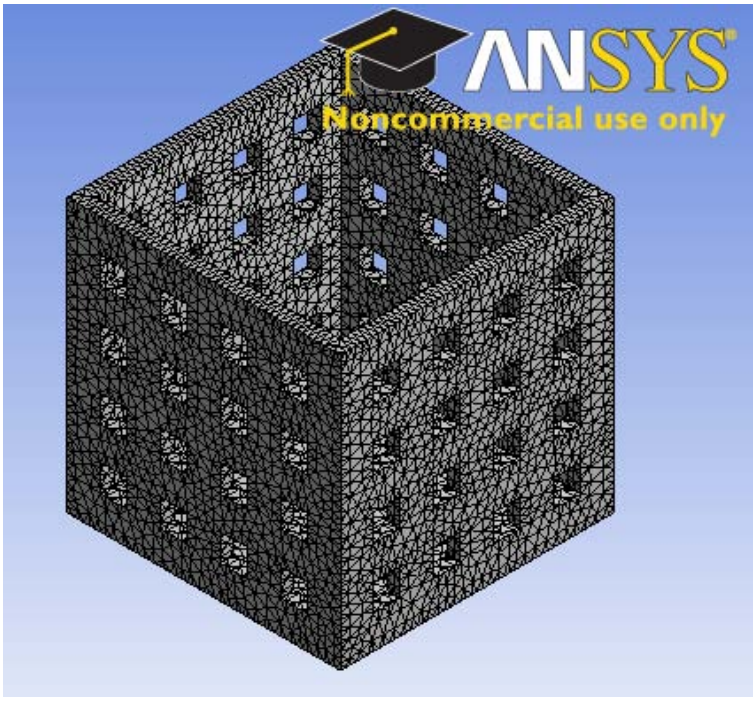

Figure 8. Finite element mesh of the CS2 lattice structure.

The linear buckling loads were computed from the finite element analysis for both of the CubeSat structures. Both cubic structures were fabricated with some walls in the R0B90 mode and other walls in the R90B0 mode as sketched in Figure 7. Here "R" indicates the Raster direction, i.e. the extrusion direction from the tip of the 3-D printer while 'B" is the Build direction such that each layer is built. As a result, the elastic modulus is different depending on in which mode the wall is fabricated. For R0B90 walls, the average elastic modulus in compression from the test data is 2.81 GPa while that for R90B90 is 2.64 GPa.

The present analyses used either one of the modulus or the average modulus of the two, respectively, in order to see the range of the buckling loads. The buckling loads are tabulated in Tables 3 and 4, respectively. The results for solid wall cubes (CS1 structure) were well predicted using the buckling load. Especially, when the maximum elastic modulus was utilized, the finite element result over-predicted the experimental failure load. On the other hand, using the minimum elastic modulus resulted in the under-prediction of the failure load. The average value of the elastic modulus yielded the best prediction.

The predicted results for the lattice-shaped wall cube (CS2 structure) were quite different from the experimental value. The linear buckling analysis does not accurately predict the failure load with stress concentration because the square holes of the lattice-shape wall cube yield stress concentrations. Consistent under prediction of the finite element analysis results was considered to be from the difference between the actual and nominal dimension of the cube. The finite element model used the nominal dimensions while the actual dimensions seemed to be slightly greater than the nominal dimensions. Because the purpose of these analyses to understand the predictive models rather than prediction of exact failure loads, any further refined analyses were not conducted. However, these finite element analyses suggest some guidelines to model the CubeSat structures in order to predict failure strength under compression. Future simulations will incorporate the anisotropy in elastic modulus evidenced in the data from section II.

Table 3. Predicted Failure Loads from Linear Buckling Analysis for Solid Wall Cube (CS1 structure)

	E = 2.64 GPa	E = 2.73 GPa	E = 2.81 GPa
Predicted Failure Load	59.0 KN	64.2 KN	66.1 KN
Experimental Failure Load	62.1 KN	64.9 KN	64.9 KN
Error (%)	-4.30	-1.03	1.87

Table 4. Predicted Failure Loads from Linear Buckling Analysis for Lattice-shape Wall Cube (CS2 structure)

	E = 2.64 GPa	E = 2.73 GPa	E = 2.81 GPa
Predicted Failure Load	33.5 KN	35.8 KN	38.0 KN
Experimental Failure Load	40.6 KN	40.6 KN	40.6 KN
Error (%)	-17.52	-11.8	-6.56

IV. Support of the DARPA Digital Manufacturing, Analysis, Correlation, and Estimation (DMACE) Challenge

The DMACE Challenge highlighted the capabilities of digital manufacturing and expanded the understanding of the science involved. NPS digitally manufactured several complex structures and conducted a series of structural load tests upon them. Data from the manufacture and load tests were posted on the DARPA-DMACE website (https://www.dmace.net/). The DMACE Challenge invited participants from around the world to predict the failure loads of DDM titanium spheres and polycarbonate CubeSats based upon input data about the processing and geometry of the test structures. Participant models were evaluated by their ability to predict the test results of the final DDM structures.

The polycarbonate portion of the DMACE Challenge was hosted by the Naval Postgraduate School and consisted of three phases of data. The first phase of data was the basic processing-mechanical property relationships in compression and tension described in section II. The second phase of the data was termed "training data" and was comprised of the data for the CS1 and CS2 structures described in section III of this report. The final phase of data was for the final challenge geometry upon which the participants of the DMACE Challenge were evaluated.

The objective of the DMACE Challenge final geometry (CSF) was to predict the crushing load for a CubeSat structure with a complex internal structure. The chosen geometry was a four-sided cube shell with 5 mm thick walls and an interior spiral web that swept 45 deg such that the attachment at the base is at the middle of the cube sides and the attachment at the top was at the corners. (Figure 9) Figure 9A shows the overall dimensions of the cube structure. Figures 9B and 9C show the top view of the structure at the left and the bottom view at the right. The part was built with raster lines as noted in the drawing (from left to right). Computer Aided Design (CAD) files were provided to participants in three CAD file formats, IGES, STEP AP203, and STEP AP214, to remove any ambiguity in the structure's geometry.

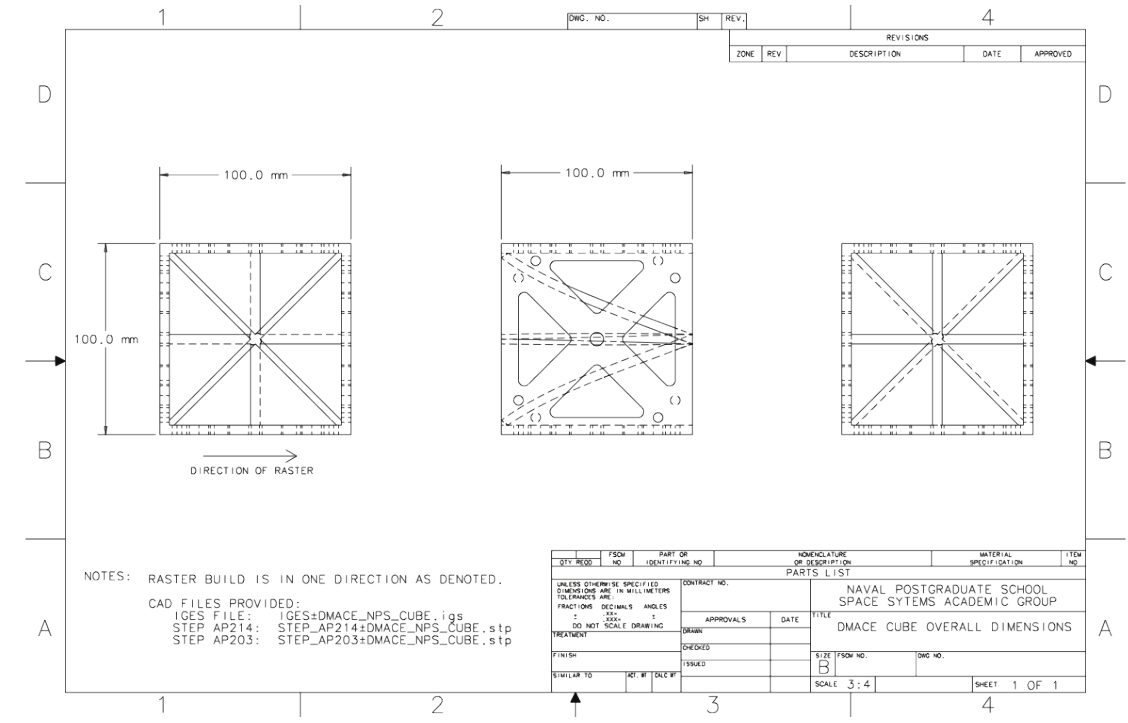

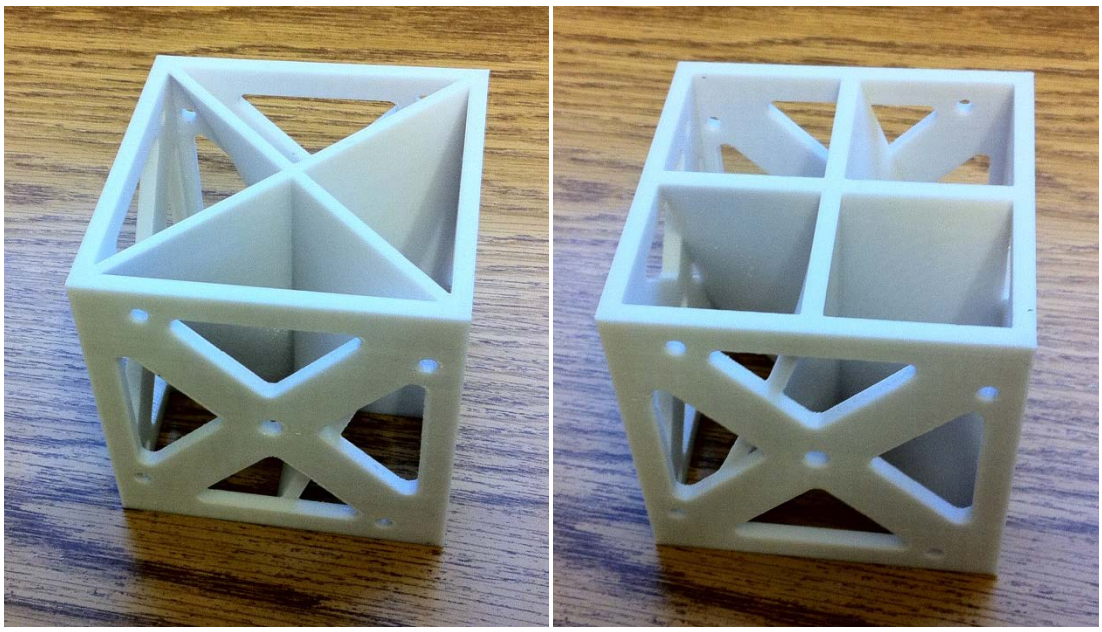

Figure 9. Geometry (top) of the final CubeSat Geometry. Photgraphs of the bottom (left image) and top (right image) of the DDM-produced CubeSat.

During the challenge, a detailed description of the swept interior webs was provided in response to participant questions concerning the tapered thickness of the webs. The description provided was as follows:

"*Construction of the Spiral Webs:*

The internal spiral webs were constructed by first creating a single 2D swept surface as one of the blades, from the center of the cube to the outside surface. The surface is swept such that it intersects the bottom plane of the cube from the center to the middle of the outside edge; and intersects the top plane of the cube from the center to the corner.
This single surface is copied and translated along the direction of the cube edge, plus and minus 2.5 mm to form a web thickness of 5 mm at the base. This results in a web thickness at the top of 3.5 mm (5mm x cos(45 deg)).
Four new surfaces were defined by the eight corners of the two outer surfaces, and the six surfaces stitched together to form a solid spiral web. The spiral solid web is then copy-rotated to create the four spiral webs and ultimately joined with the cube shell."

The crushing load of the final CubeSat geometry, CSF, was determined using the same instrumentation as described above for the CS1 and CS2 structures. The crushing load was taken to be the maximum force during compression. The load displacement curve for the CSF structure was different from the CS1 and CS2 structures in that there was no well-defined yield point in the load-displacement curve. Strong serrations were apparent near the maximum load, as seen in the CS1 structure. The final failure was brittle as was the case for the CS1 and CS2 structures. The CSF structure was tested five times for the DARPA DMACE challenge to provided sufficient statistics. The final values can be seen in Table 5. The mean crushing load was 58.7kN with a standard deviation of 2.7kN, which was less than 5 percent of the mean value.

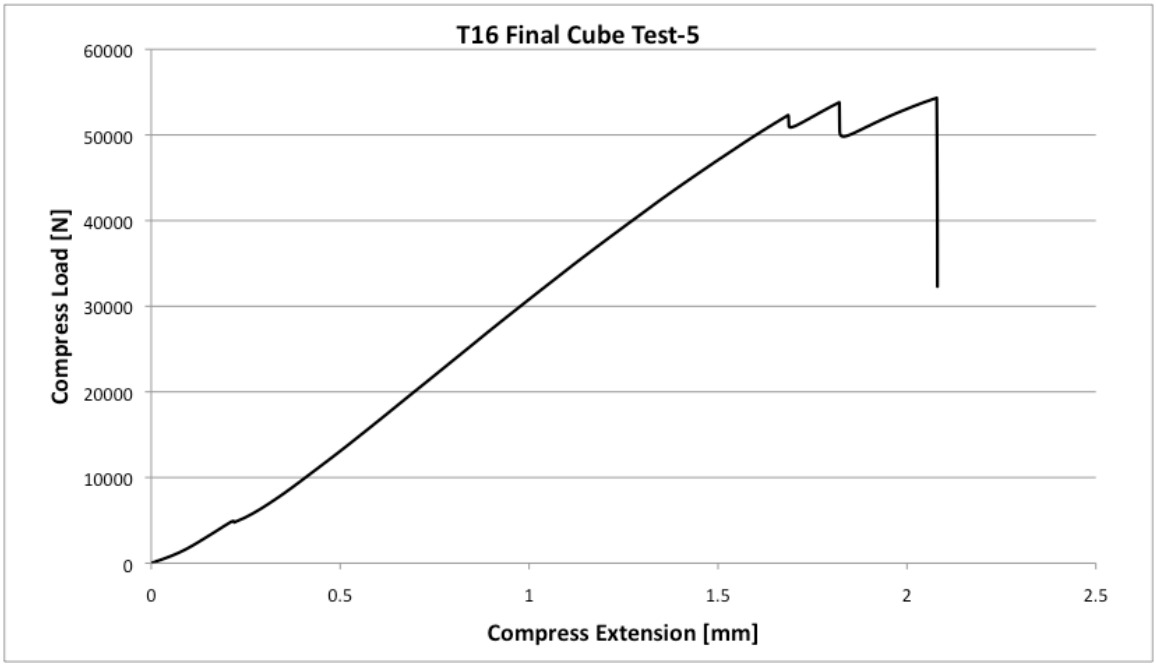

Figure 10. Load-displacement curve for the final CubeSat geometry test.

Table 5. Crushing load values for final five CubeSats

Sample Name	Max. Compress Load (N)
T16 Final Cube Test-1	60167.3
T16 Final Cube Test-2	61589.6
T16 Final Cube Test-3	58954.8
T16 Final Cube Test-4	58363.8
T16 Final Cube Test-5	54317.5

V. Conclusions

This DARPA project has completed several objectives in order to better understand and control DDM of complex, polycarbonate structures. We have performed a detailed, parametric study of the processing-property relationships in the polycarbonate polymer system. We were able to identify both statistically significant and insignificant factors in these relationships. Response surfaces were generated from these results that can be used to predict the changes in material mechanical properties as a function of processing parameters. Based upon these results, we fabricated, predicted, and tested the mechanical behavior of larger, more complex structures. Finite element analysis was able to successfully predict the compressive strength of some structures, while identifying weaknesses in this approach for others. Finally, we supported the DARPA DMACE Challenge and used it as a vehicle for assessing our ability to successfully predict the mechanical behavior of digitally manufactured, complex structures.

THIS PAGE INTENTIONALLY LEFT BLANK

References

1. Verne, J., *Twenty Thousand Leagues under the Sea*. The Extrordinary Voyages1870: P.J. Hetzel.
2. Wendel, B., et al., *Additive Processing of Polymers.* Macromol. Mater. Eng., 2008. **293**(10): p. 799-809.
3. Evans, R.S., et al., *Rapid Manufacturing of Silicon Carbide Composites.* Rapid Prototyping Journal, 2005. **11**(1): p. 37-40.
4. Masood, S.H. and W.Q. Song, *Thermal Characteristics of a New Metal/Polymer Material for Fdm Rapid Prototyping Process.* Assembly Automation, 2005. **25**(4): p. 309-315.
5. Sood, A.K., R.K. Ohdar, and S.S. Mahapatra, *Parametric Appraisal of Mechanical Property of Fused Deposition Modelling Processed Parts.* Materials & Design, 2010. **31**(1): p. 287-295.
6. Ahn, S.-H., et al., *Anisotropic Material Properties of Fused Deposition Modeling Abs.* Rapid Prototyping Journal, 2002. **8**(4): p. 248-257.
7. Masood, S.H., K. Mau, and W.Q. Song, *Masood_Matsciforum_2010.* Materials Science Forum, 2010. **654-656**: p. 2556-2559.
8. International, A., *Standard Test Method for Compressive Properties of Rigid Plastics: D695*, 2010: New York, NY. p. 7.
9. International, A., Standard Test Method for Tensile Properties of Plastics: D638, 2010: New York, NY. p. 16.

THIS PAGE INTENTIONALLY LEFT BLANK

Appendix A: Mechanical Testing Data

Table A.1 T12 compression test result

Sample Number	Young's Modulus (GPa)	Maximum Stress (MPa)
T12R0B0-1	2.91	76.08
T12R0B0-2	2.82	75.76
T12R0B0K-1	3.08	77.63
T12R0B0K-2	3.01	77.91
T12R90B0-1	2.64	61.26
T12R90B0-2	2.38	62.2
T12R90B0K-1	2.54	63.59
T12R90B0K-2	2.48	64.06
T12R90B90-1	2.59	57.23
T12R90B90-2	2.59	57.03
T12R90B90K-1	2.64	59.07
T12R90B90K-2	2.68	59.49
T12R0B90-1	2.54	56.66
T12R0B90-2	2.58	57.62
T12R0B90K-1	2.64	59.14
T12R0B90K-2	2.66	59.91

Table A.2 T16 compression test result

Sample Number	Young's Modulus (GPa)	Maximum Stress (MPa)
T16R0B0-1	2.93	72.24
T16R0B0-2	2.82	73.23
T16R0B0K-1	2.89	71.44
T16R0B0K-2	2.88	72.59
T16R90B0-1	2.65	68.71
T16R90B0-2	2.60	68.16
T16R90B0K-1	2.62	68.90
T16R90B0K-2	2.66	66.87
T16R90B90-1	2.61	66.97
T16R90B90-2	2.67	64.65
T16R90B90K-1	2.68	67.24
T16R90B90K-2	2.66	67.44
T16R0B90-1	2.81	67.99
T16R0B90-2	2.81	66.12
T16R0B90K-1	2.51	60.08
T12R0B90K-2	2.85	65.58

Table A.3 Tensile test result

Sample Number	Young's Modulus (GPa)	Maximum Stress (MPa)
T16R0B0-1	1.28	63.04
T16R0B0-2	1.29	62.5
T16R90B0-1	1.15	49.4
T16R90B0-2	1.2	50.71
T16R90B90-1	1.08	21.03
T16R90B90-2	1.08	20.23
T16R0B90-1	1.11	20.92
T16R0B90-2	1.11	26.39

Appendix B: Statistical Analysis

Compression Data, All Factors in Model:

Least Squares Fit: Young Modulus
Actual by Predicted Plot

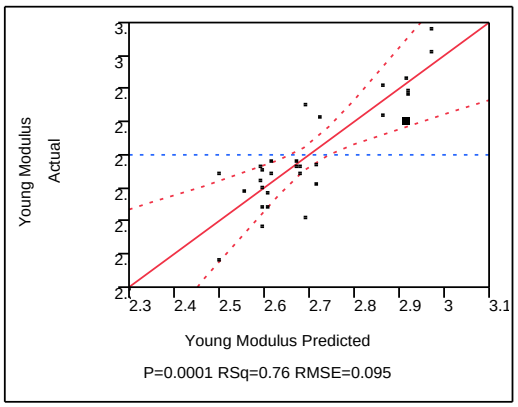

Summary of Fit

RSquare	0.763773
RSquare Adj	0.651284
Root Mean Square Error	0.09501
Mean of Response	2.700938
Observations (or Sum Wgts)	32

Analysis of Variance

Source	DF	Sum of Squares	Mean Square	F Ratio
Model	10	0.61290625	0.061291	6.7897
Error	21	0.18956562	0.009027	**Prob > F**
C. Total	31	0.80247187		0.0001*

Parameter Estimates

Term	Estimate	Std Error	t Ratio	Prob>|t|
Intercept	2.7009375	0.016796	160.81	<.0001*
Tip Size(0.178,0.254)	0.0271875	0.016796	1.62	0.1204
Raster Angle(0,90)	-0.095313	0.016796	-5.67	<.0001*
Build Angle(0,90)	-0.043438	0.016796	-2.59	0.0172*
Bake[no bake]	-0.016563	0.016796	-0.99	0.3353
Tip Size*Raster Angle	0.0109375	0.016796	0.65	0.5220
Tip Size*Build Angle	0.0153125	0.016796	0.91	0.3723
Tip Size*Bake[no bake]	0.0259375	0.016796	1.54	0.1375
Raster Angle*Build Angle	0.0778125	0.016796	4.63	0.0001*
Raster Angle*Bake[no bake]	0.0021875	0.016796	0.13	0.8976
Build Angle*Bake[no bake]	0.0090625	0.016796	0.54	0.5952

Effect Tests

Source	Nparm	DF	Sum of Squares	F Ratio	Prob > F
Tip Size(0.178,0.254)	1	1	0.02365312	2.6203	0.1204
Raster Angle(0,90)	1	1	0.29070313	32.2040	<.0001*
Build Angle(0,90)	1	1	0.06037813	6.6887	0.0172*
Bake	1	1	0.00877813	0.9724	0.3353
Tip Size*Raster Angle	1	1	0.00382813	0.4241	0.5220

Source	Nparm	DF	Sum of Squares	F Ratio	Prob > F
Tip Size*Build Angle	1	1	0.00750312	0.8312	0.3723
Tip Size*Bake	1	1	0.02152813	2.3849	0.1375
Raster Angle*Build Angle	1	1	0.19375313	21.4639	0.0001*
Raster Angle*Bake	1	1	0.00015312	0.0170	0.8976
Build Angle*Bake	1	1	0.00262812	0.2911	0.5952

Response maximum stress

Actual by Predicted Plot

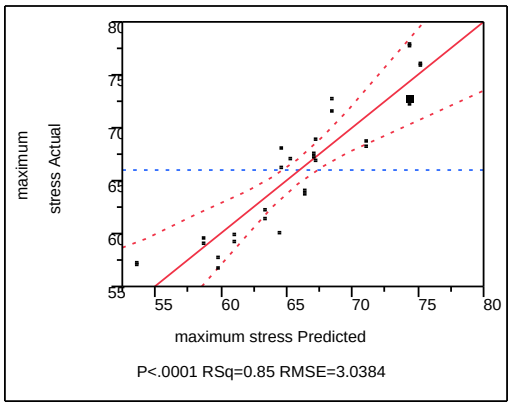

Summary of Fit

RSquare	0.847904
RSquare Adj	0.775477
Root Mean Square Error	3.03838
Mean of Response	65.92719
Observations (or Sum Wgts)	32

Analysis of Variance

Source	DF	Sum of Squares	Mean Square	F Ratio
Model	10	1080.7675	108.077	11.7071
Error	21	193.8668	9.232	**Prob > F**
C. Total	31	1274.6342		<.0001*

Parameter Estimates

Term	Estimate	Std Error	t Ratio	Prob>|t|
Intercept	65.927188	0.537115	122.74	<.0001*
Tip Size(0.178,0.254)	1.8871875	0.537115	3.51	0.0021*
Raster Angle(0,90)	-3.000937	0.537115	-5.59	<.0001*
Build Angle(0,90)	-3.377812	0.537115	-6.29	<.0001*
Bake[no bake]	-0.451563	0.537115	-0.84	0.4100
Tip Size*Raster Angle	0.5478125	0.537115	1.02	0.3194
Tip Size*Build Angle	2.3934375	0.537115	4.46	0.0002*
Tip Size*Bake[no bake]	0.6084375	0.537115	1.13	0.2701
Raster Angle*Build Angle	1.4090625	0.537115	2.62	0.0159*
Raster Angle*Bake[no bake]	-0.975938	0.537115	-1.82	0.0835
Build Angle*Bake[no bake]	-0.506562	0.537115	-0.94	0.3563

Effect Tests

Source	Nparm	DF	Sum of Squares	F Ratio	Prob > F
Tip Size(0.178,0.254)	1	1	113.96725	12.3451	0.0021*
Raster Angle(0,90)	1	1	288.18003	31.2162	<.0001*
Build Angle(0,90)	1	1	365.10775	39.5491	<.0001*

Source	Nparm	DF	Sum of Squares	F Ratio	Prob > F
Bake	1	1	6.52508	0.7068	0.4100
Tip Size*Raster Angle	1	1	9.60315	1.0402	0.3194
Tip Size*Build Angle	1	1	183.31338	19.8568	0.0002*
Tip Size*Bake	1	1	11.84628	1.2832	0.2701
Raster Angle*Build Angle	1	1	63.53463	6.8822	0.0159*
Raster Angle*Bake	1	1	30.47853	3.3015	0.0835
Build Angle*Bake	1	1	8.21138	0.8895	0.3563

Compression Data, Maximum Stress Model with Bake parameter and Tip size-raster angle interaction removed:

Response maximum stress
Actual by Predicted Plot

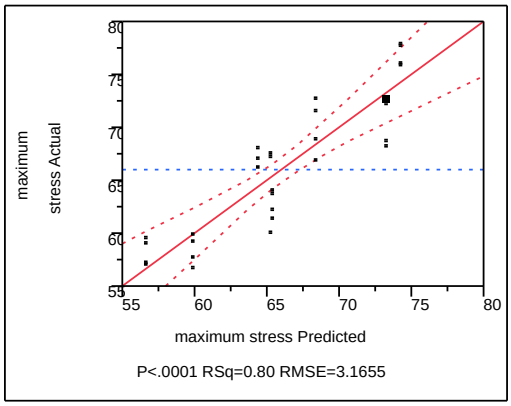

Summary of Fit

RSquare	0.795603
RSquare Adj	0.756296
Root Mean Square Error	3.165506
Mean of Response	65.92719
Observations (or Sum Wgts)	32

Analysis of Variance

Source	DF	Sum of Squares	Mean Square	F Ratio
Model	5	1014.1030	202.821	20.2407
Error	26	260.5312	10.020	**Prob > F**
C. Total	31	1274.6342		<.0001*

Lack Of Fit

Source	DF	Sum of Squares	Mean Square	F Ratio
Lack Of Fit	2	147.50768	73.7538	15.6613
Pure Error	24	113.02352	4.7093	**Prob > F**
Total Error	26	260.53121		<.0001*
				Max RSq
				0.9113

Parameter Estimates

Term	Estimate	Std Error	t Ratio	Prob>|t|
Intercept	65.927188	0.559588	117.81	<.0001*
Tip Size(0.178,0.254)	1.8871875	0.559588	3.37	0.0023*
Raster Angle(0,90)	-3.000937	0.559588	-5.36	<.0001*
Build Angle(0,90)	-3.377812	0.559588	-6.04	<.0001*
Tip Size*Build Angle	2.3934375	0.559588	4.28	0.0002*
Raster Angle*Build Angle	1.4090625	0.559588	2.52	0.0183*

Compression Data, Young's Modulus Model with Bake and tip size parameters removed:

Actual by Predicted Plot

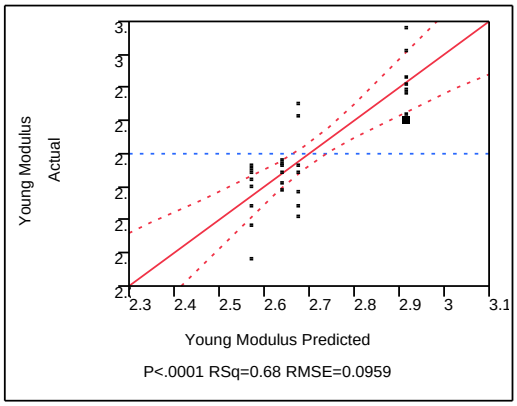

Summary of Fit

RSquare	0.678945
RSquare Adj	0.644546
Root Mean Square Error	0.095924
Mean of Response	2.700938
Observations (or Sum Wgts)	32

Analysis of Variance

Source	DF	Sum of Squares	Mean Square	F Ratio
Model	3	0.54483438	0.181611	19.7375
Error	28	0.25763750	0.009201	**Prob > F**
C. Total	31	0.80247187		<.0001*

Parameter Estimates

Term	Estimate	Std Error	t Ratio	Prob>|t|
Intercept	2.7009375	0.016957	159.28	<.0001*
Raster Angle(0,90)	-0.095313	0.016957	-5.62	<.0001*
Build Angle(0,90)	-0.043438	0.016957	-2.56	0.0161*
Raster Angle*Build Angle	0.0778125	0.016957	4.59	<.0001*

Tension Data, All Factors in Model:

Least Squares Fit Response Max Stress (MPa)
Actual by Predicted Plot

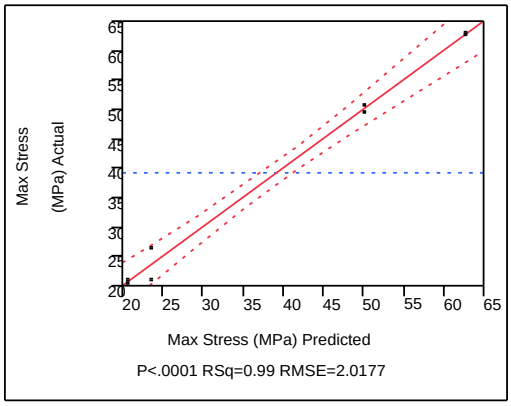

Summary of Fit

RSquare	0.993579
RSquare Adj	0.988763
Root Mean Square Error	2.017691
Mean of Response	39.2775
Observations (or Sum Wgts)	8

Analysis of Variance

Source	DF	Sum of Squares	Mean Square	F Ratio
Model	3	2519.6877	839.896	206.3081
Error	4	16.2843	4.071	**Prob > F**
C. Total	7	2535.9719		<.0001*

Parameter Estimates

Term	Estimate	Std Error	t Ratio	Prob>|t|
Intercept	39.2775	0.713361	55.06	<.0001*
Raster Angle	-3.935	0.713361	-5.52	0.0053*
Build Angle	-17.135	0.713361	-24.02	<.0001*
Raster Angle*Build Angle	2.4225	0.713361	3.40	0.0274*

Response Young's Modulus (GPa)
Actual by Predicted Plot

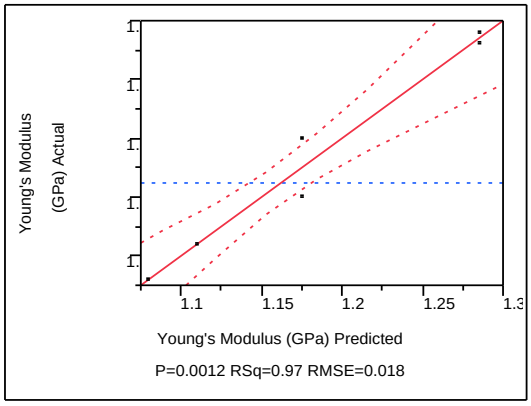

Summary of Fit

RSquare	0.974384
RSquare Adj	0.955172
Root Mean Square Error	0.018028
Mean of Response	1.1625
Observations (or Sum Wgts)	8

Analysis of Variance

Source	DF	Sum of Squares	Mean Square	F Ratio
Model	3	0.04945000	0.016483	50.7179
Error	4	0.00130000	0.000325	**Prob > F**
C. Total	7	0.05075000		0.0012*

Parameter Estimates

Term	Estimate	Std Error	t Ratio	Prob>|t|
Intercept	1.1625	0.006374	182.39	<.0001*
Raster Angle	-0.035	0.006374	-5.49	0.0054*
Build Angle	-0.0675	0.006374	-10.59	0.0004*
Raster Angle*Build Angle	0.02	0.006374	3.14	0.0349*

INITIAL DISTRIBUTION LIST

1. Defense Technical Information Center
   Ft. Belvoir, Virginia

2. Dudley Knox Library
   Naval Postgraduate School
   Monterey, California

3. Research Sponsored Programs Office, Code 41
   Naval Postgraduate School
   Monterey, CA 93943

4. Distinguished Professor Young W. Kwon
   Naval Postgraduate School
   Monterey, CA 93943

5. Associate Professor Luke N. Brewer
   Naval Postgraduate School
   Monterey, CA 93943

6. Professor Rudolf Panholzer
   Naval Postgraduate School
   Monterey, CA 93943

7. Dr. Chanman Park
   Naval Postgraduate School
   Monterey, CA 93943

8. Dr. Dan Sakoda
   Naval Postgraduate School
   Monterey, CA 93943

9. LtCol. Timothy Sands
   Naval Postgraduate School
   Monterey, CA 93943